Supporting Information

Multispectral Nanoparticle Tracking Analysis for the Real-Time and Label-Free Characterization of Amyloid-β Self-Assembly in vitro

Colman Moore[1], Ryan Wing[1], Timothy Pham[1], and Jesse V Jokerst[1,2,3*]

1. Department of NanoEngineering
2. Materials Science and Engineering Program
3. Department of Radiology

University of California, San Diego. La Jolla, CA 92093. United States.
jjokerst@eng.ucsd.edu

Table of Contents.

Particle Type	Laser	Gain (mW)	Exposure (ms)	Particle Ratio (90: 490: 1000)	Laser	Gain (mW)	Exposure (ms)
PSL-90	R	40	15	10:5:1	R	24	15
PSL-90	G	40	15	10:5:1	G	24	15
PSL-90	B	40	15	10:5:1	B	24	15
PSL-90	RGB	40	15	10:5:1	RGB	24	15
PSL-490	R	11	15	1:1:1	R	24	31
PSL-490	G	11	15	1:1:1	G	24	31
PSL-490	B	11	15	1:1:1	B	24	31
PSL-490	RGB	4	15	1:1:1	RGB	24	31
PSL-1000	R	15	15	1:5:10	R	6	32
PSL-1000	G	15	15	1:5:10	G	6	32
PSL-1000	B	15	15	1:5:10	B	0	32
PSL-1000	RGB	5	15	1:5:10	RGB	0	32

Table S1. Acquisition settings for PSL particle measurements. Blue (445 nm), green (520 nm), and red (635 nm) wavelengths were used for all samples. Gain and exposure settings were adjusted on a per-sample basis to maximize the number of focused particles on the screen while minimizing noise from highly scattering particles. These settings were matched between samples of the same composition when possible. The theoretical concentrations (diluted from the stock values provided by the supplier) for the PSL mixtures were as follows: 10:5:1 (90-nm: 490-nm: 1000-nm) = 6.7E7 mL^{-1}, 3.3E7 mL^{-1}, 6.7E6 mL^{-1}. 1:1:1 = 1.25E7 mL^{-1}, 1.25E7 mL^{-1}, 1.25E7 mL^{-1}. 1:5:10 = 5.0E6 mL^{-1}, 2.5E7 mL^{-1}, 5.0E7 mL^{-1}.

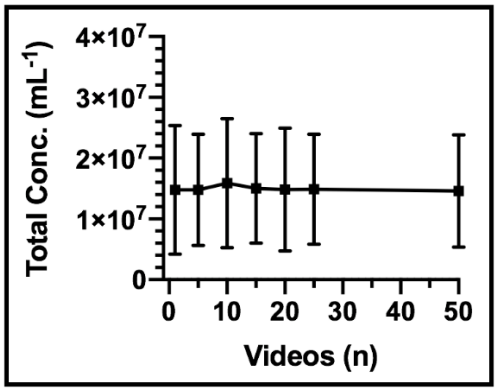

Figure S1. Effect of video number on total measured aggregate concentration. Total concentration was measured with MNTA for 5 μM $A\beta_{1\text{-}42}$ after solubilizing in 40 mM Tris for increasing numbers of recorded videos (n = 3, error bars = SEM).

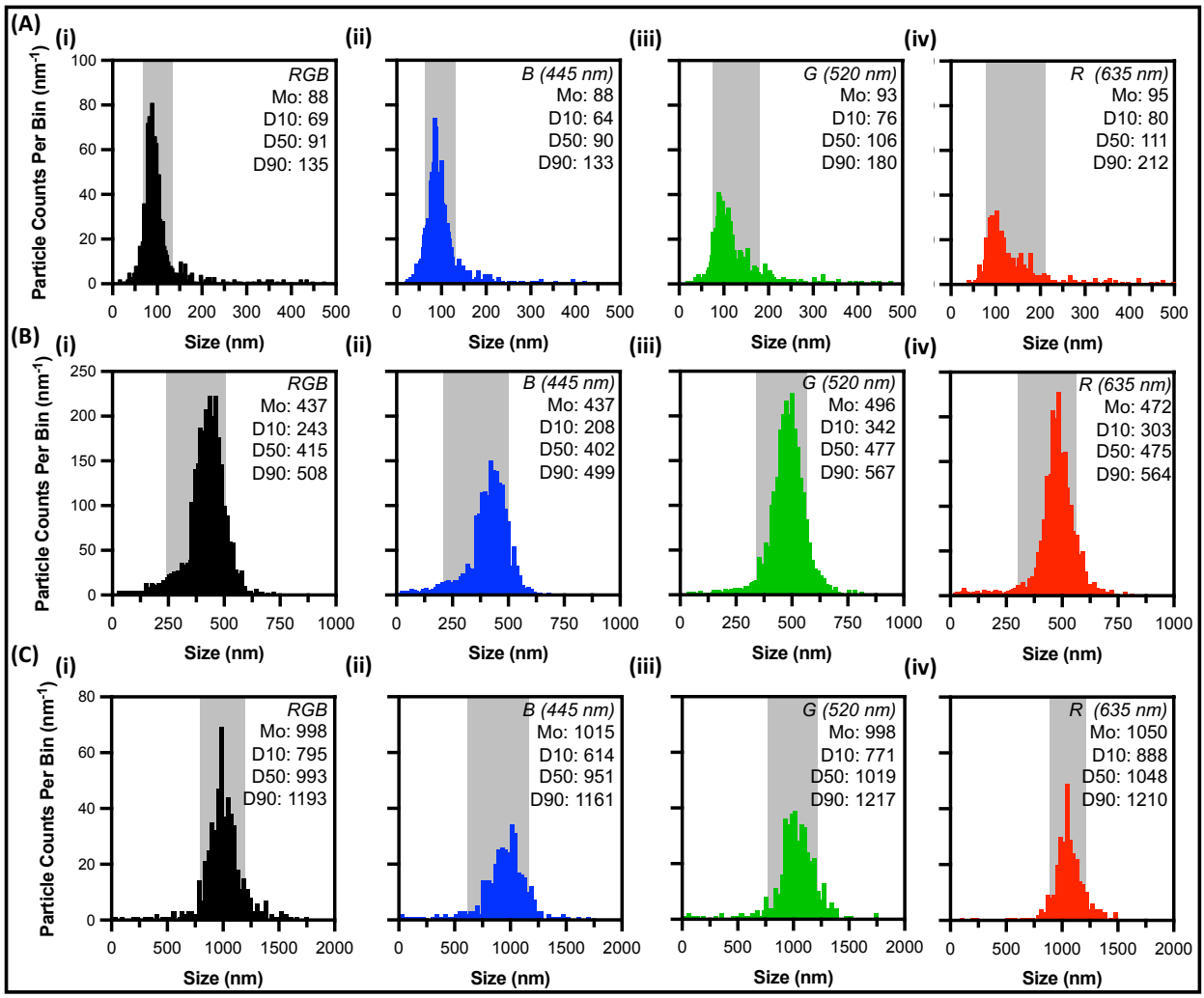

Figure S2. Multispectral versus monospectral excitation for NTA of monomodal PSL spheres (nominal diameters: 90 nm, 490 nm, and 1,000 nm). Size distributions of nominal (**A**) 90-nm PSL spheres, (**B**) 490-nm PSL spheres, and (**C**) 1,000-nm PSL spheres measured with (**i**) three lasers: red (635 nm, 8 mW), green (520 nm, 12 mW), and blue (445 nm, 70 mW), (**ii**) blue only (445 nm, 70 mW), (**iii**) green only (520 nm, 12 mW), and (**iv**) red only (635 nm, 8 mW). The modal particle size (Mo) is shown for each distribution. D10, D50, and D90 values refer to the size that 10%, 50%, and 90% of measured particles fall below. Shaded regions indicate the D10 (left edge) and D90 (right edge) values. These plots demonstrate the dependence of both the width of the size distribution and the number of particle counts on wavelength choice.

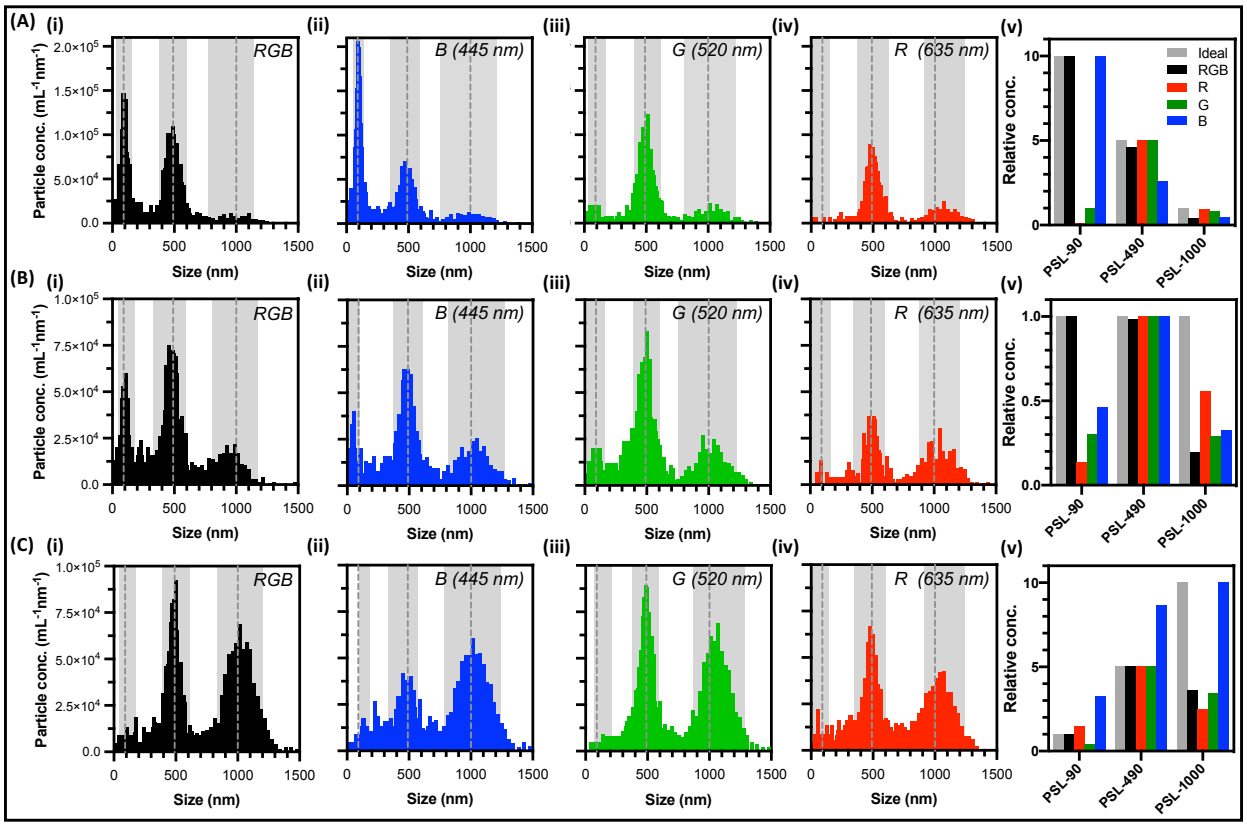

Figure S3. Multispectral versus monospectral excitation for NTA of trimodal mixtures of PSL spheres (nominal diameters: 90 nm, 490 nm, and 1,000 nm). Size distributions of PSL mixtures with relative concentration ratios of (**A**) 10: 5: 1 (90-nm: 490-nm: 1000-nm), (**B**) 1: 1: 1, and (**C**) 1: 5: 10 measured with (**i**) three lasers: red (635 nm, 8 mW), green (520 nm, 12 mW), and blue (445 nm, 70 mW), (**ii**) blue only (445 nm, 70 mW), (**iii**) green only (520 nm, 12 mW), and (**iv**) red only (635 nm, 8 mW). The dashed line in each panel corresponds to the nominal diameter of the particle subpopulation. The shaded regions approximate the particle counts attributable to a given particle subpopulation. These boundaries were applied by taking the modal size of the subpopulation and adding/subtracting one standard deviation of the size distribution as measured for its respective monomodal sample (**Fig. S2**). The particle counts in each shaded region were summed and normalized for comparison to the ideal ratio in panel (**v**) of each row.

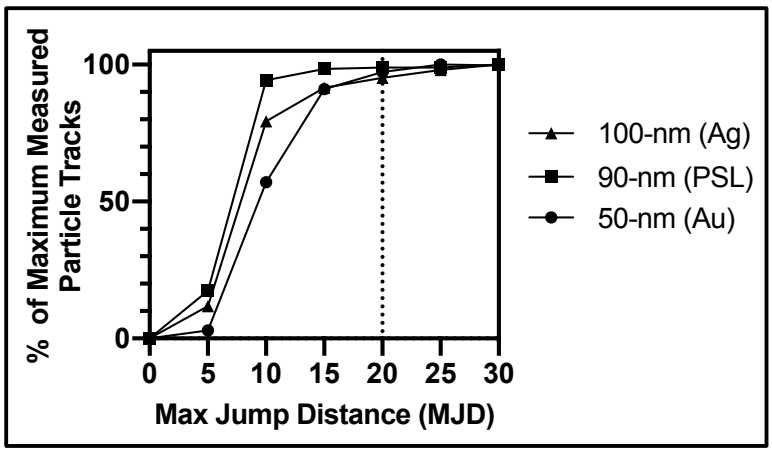

Figure S4. Detection of small nanoparticles as a function of max jump distance (MJD). Commercially available nanoparticle standards with average diameters of 50 nm (Au), 90 nm (PSL), and 100 nm (Ag) were used to determine a reasonable value for the MJD for routine analysis of polydisperse Aβ solutions containing small (<100 nm) aggregates. The size distribution of each particle type was measured for a range of MJDs from 0-30 pixels (camera calibration constant = 190 nm/pix). The number of particle counts for each distribution (at each MJD) was recorded and each value was normalized to the count for a MJD of 30 pixels, where a plateau in the measured counts was observed. The dotted line at MJD = 20 corresponds to the value used for Aβ experiments in this work. This data indicates that an MJD of 20 was sufficient for detecting 97 ± 2% of diffusing particles/aggregates in the 50 – 100 nm size range for a given sample.

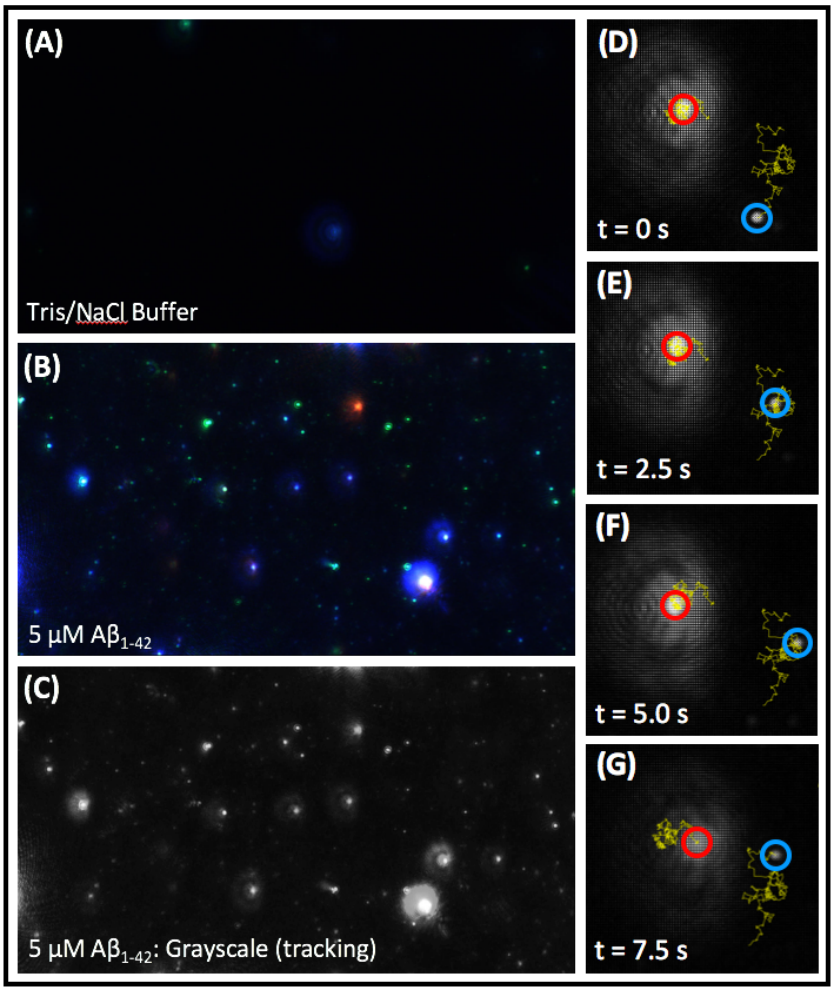

Figure S5. Principle of MNTA for Aβ sizing via Brownian dynamics. (**A**) Color video-frame from MNTA showing the minimal scattering from background particles in aggregation buffer (40 mM Tris, pH 8.0, 150 mM NaCl). (**B**) Color video-frame showing the multispectral scattering of aggregates in solution after addition of 5 µM Aβ. The variety of scattering intensities from the red (635 nm), green (520 nm), and blue (445 nm) lasers is due to the polydispersity of the Aβ aggregates and the wavelength to particle size scattering dependence. (**C**) The same video-frame as (**B**) after conversion to 8-bit grayscale—these grayscale videos are used for tracking analysis. (**D-G**) A magnification of (**C**) is presented to illustrate the different track lengths of two diffusing particles over time: (**D**) t = 0 s, (**E**) t = 2.5 s, (**F**) t = 5.0 s, and (**G**) t = 7.5 s. A larger particle—indicated by the red circle and higher scattering intensity—diffuses more slowly than a smaller particle (blue circle). Their path lengths are traced in yellow and illustrate their size-dependent diffusivities.

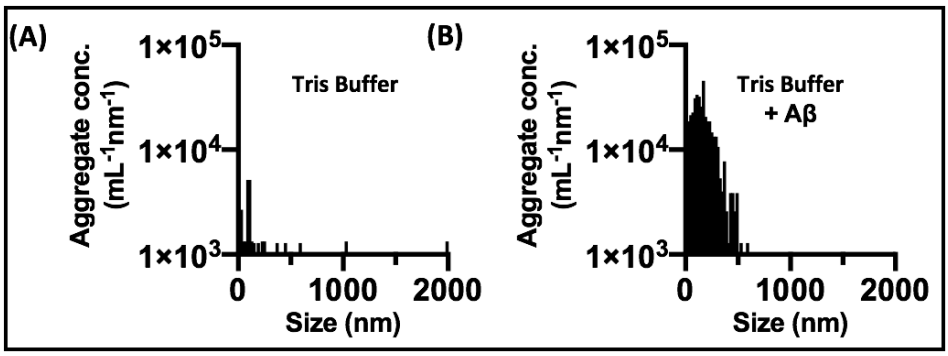

Figure S6. Comparison of the measured size distribution for buffer (Tris 40 mM, NaCl 150 mM) before and after addition of $A\beta_{1-42}$. (A) Size distribution for aggregation buffer measured with MNTA**.** The total concentration detected for buffer was 1.6E6 particles/mL, where only 30% of counts were in the 20-2,000 nm range (5.9E5 particles/mL). In contrast, 98±2% of counts from Aβ samples (n=5) were in the 20-2,000 nm range. **(B)** Representative size distribution for 5 μM $A\beta_{1-42}$ at t = 0 h. The average concentration was 5.4E6 particles/mL between 20-2,000 nm, 9-fold higher than in buffer.

(A)

% Glycerol	Theoretical Visc. (cP)
0	0.85343
5%	0.99155
10%	1.1616
15%	1.3734
20%	1.6403
25%	1.9813
30%	2.4235

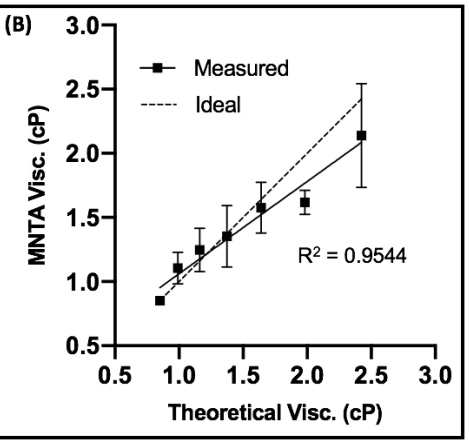

Figure S7. Evaluation of viscosity measurements using MNTA. (**A**) The true viscosities of water-glycerol mixtures are theoretically known (adapted from Volk and Kähler)[1] and are presented for reference. (**B**) Monomodal PSL particles (nominal 90-nm diameter) were diluted to a concentration of 2.5E8 mL^{-1} in glycerol-water mixtures ranging from 0-30% glycerol. The ratio of the average size measured in water to the size measured in each glycerol-water mixture was used to calculate viscosity. The theoretical viscosities were plotted with respect to the MNTA measured values (solid line). Error bars represent standard deviation of three replicates. The dashed line represents an ideal 1: 1 correlation. Average viscosities measured via MNTA were directly correlated with theoretical viscosities for glycerol-water mixtures (R^2 = 0.9544). The slope of the measured vs. theoretical viscosity curve deviated from ideality by 32% (slope of 0.72 vs. 1.00).

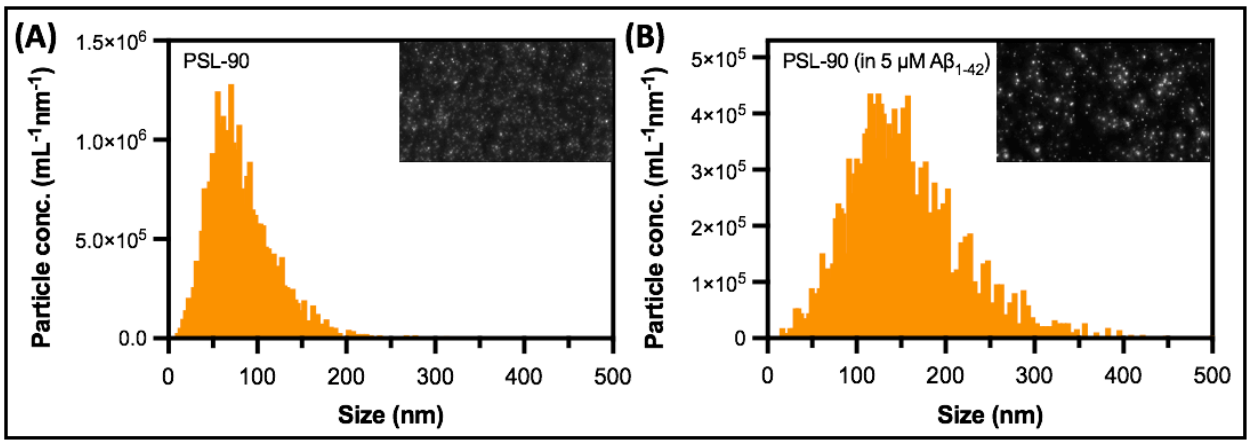

Figure S8. Determination of viscosity of $A\beta_{1-42}$ solution using MNTA. (A) Particle size distribution of PSL particles (nominal d = 90 nm) measured in water. The average size was 84 nm. A high PSL concentration (8.6E7 particles/mL measured) was used to mitigate the potential influence of Aβ aggregates on the distribution. The PSL concentration was 16-fold higher than the average particle concentration of 5 μM $A\beta_{1-42}$ in aggregation buffer (5.5E6 particles/mL). **(B)** Size distribution of the same PSL particles diluted in 5 μM $A\beta_{1-42}$ rather than water alone. The average size was 161 nm, indicating a solution of higher viscosity ($\eta = (d_2/d_1)^*\eta_{H2O,27C}$ = (161 nm/84 nm)*0.85 cP = 1.63 cP) according to the Stokes-Einstein equation.

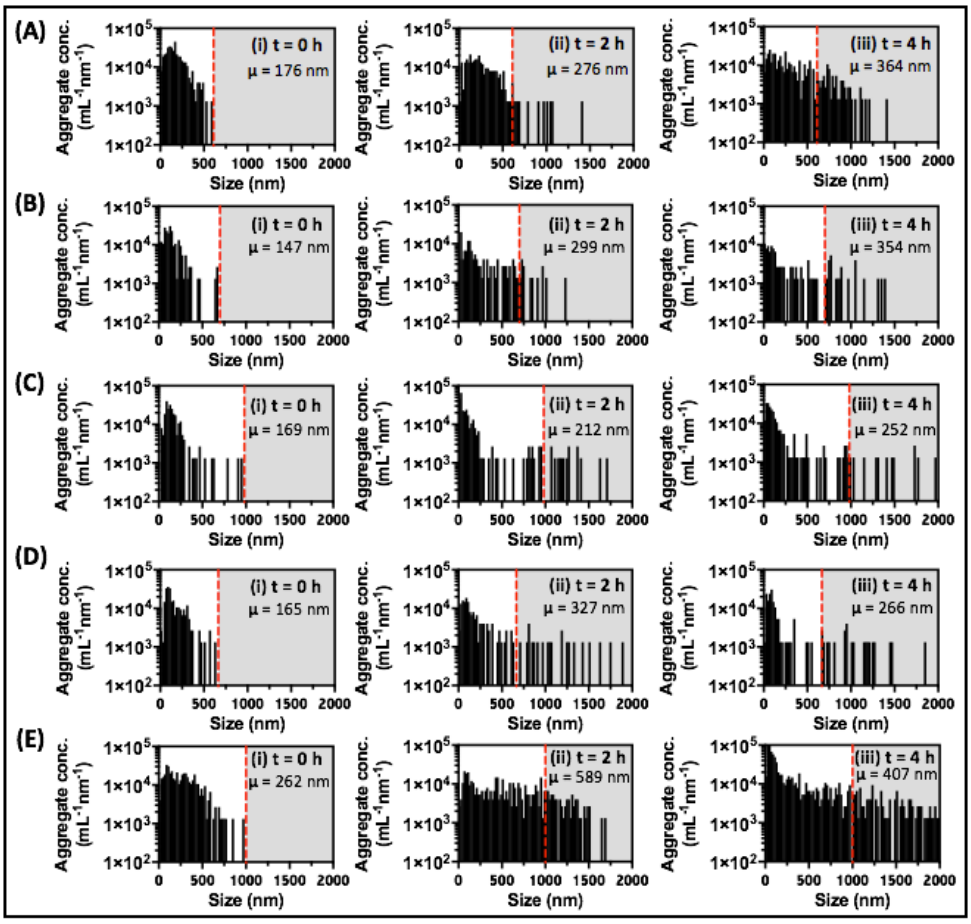

Figure S9. Individual replicates for all aggregation experiments showing size distributions at three time points. (A-E) Aggregate size distributions during the growth period corresponding to the **(A)** first, **(B)** second, **(C)** third, **(D)** fourth, and **(E)** fifth replicate experiments of monitoring $A\beta_{1\text{-}42}$ (5 μM) aggregation at t = 0, 2, and 4 h. Note: the fifth replicate was not included in Fig. 5 averaging because measurements were not recorded for the full 12 h.

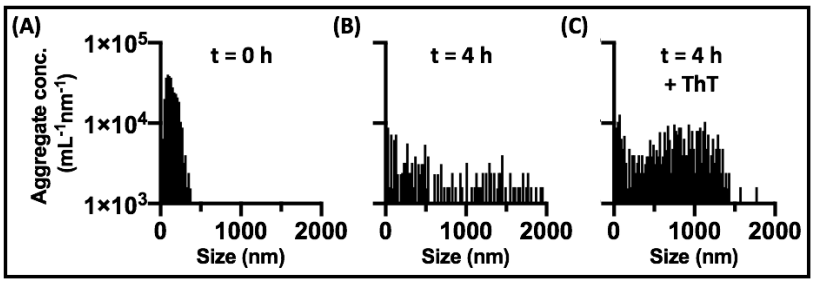

Figure S10. Effect of ThT addition on the measured size distribution of $A\beta_{1\text{-}42}$ after aggregation has already proceeded. (A) $A\beta_{1\text{-}42}$ (5 μM) size distribution after solubilizing in buffer (Tris 40 mM, NaCl 150 mM). The average size was 146 nm and the standard deviation was 43 nm. **(B)** The same sample measured after 4 h. The average size was 717 nm and the standard deviation was 572 nm. (C) ThT (10 μM) was added immediately after the t = 4 h measurement in panel B. The average size was 733 nm and the standard deviation was 410 nm. This did not have the same modulatory effect observed as when ThT was present from t = 0 h (Fig. 6C); however, an increased sensitivity to 500-1500 nm aggregates was observed.

References

1. Volk, A.; Kähler, C. J., *Experiments in Fluids* **2018,** *59* (5), 75.